Journal of the Physical Society of Japan
Vol. 67, No. 5, May, 1998, pp. 1704–1713

Impurity Scattering in Carbon Nanotubes – Absence of Back Scattering –

Tsuneya ANDO and Takeshi NAKANISHI[1]

Institute for Solid State Physics, University of Tokyo
7–22–1 Minato-ku, Roppongi, Tokyo 106

[1] *The Institute of Physical and Chemical Research (RIKEN)*
2–1 Hirosawa, Wako-shi, Saitama 351-01

(Received January 14, 1998)

The effective potential of an impurity in a $\boldsymbol{k}\cdot\boldsymbol{p}$ scheme is derived in two-dimensional graphite sheet. When the potential range is smaller than the lattice constant, it has an off-diagonal matrix element between K and K' points comparable to the diagonal element. With the increase of the range, this off-diagonal element decreases rapidly and the diagonal element for envelopes at A and B sites becomes identical. The crossover between these two regimes occurs around the range smaller than the lattice constant. In the latter regime, back scattering between states with $+k$ and $-k$ vanishes identically for the bands crossing the Fermi level in the absence of a magnetic field, leading to an extremely large conductivity. The absence of the back scattering disappears in magnetic fields, giving rise to a huge positive magnetoresistance.

KEYWORDS: graphite, carbon nanotube, fullerene tube, Landau level, magnetoresistance, effective-mass theory

§1. Introduction

A carbon nanotube (CN) consists of coaxially rolled graphite sheets.[1)] Because the distance between different sheets is much larger than the nearest neighbor carbon atoms, electronic properties of CN's are dominated by those of a single-shell CN. A single-shell CN can be either a metal or a semiconductor depending on the circumference length and the helical fashion. The purpose of this paper is to study effects of impurity scattering in CN's and demonstrate a possibility of absence of back scattering for conventional scatterers.

Various calculations have been performed to predict energy bands of CN's.[2−12)] It has been found that the characteristic properties are all reproduced quite well in a $\boldsymbol{k}\cdot\boldsymbol{p}$ method,[13,14)] which is effective in the study of effects of external fields such as magnetic and electric fields. In fact, it has been successful in the study of magnetic properties including the Aharonov-Bohm (AB) effect on the band gap,[15,16)] optical absorption spectra,[17−19)] and lattice instabilities in the presence and absence of a magnetic field.[20,21)]

Transport properties of CN's are interesting because CN's have a structure topologically different from that of conventional quantum wires fabricated using semiconductor heterostructures. There have been some reports on experimental study of transport in CN bundles.[22)] Quite recently, measurements of magnetotransport of a single nanotube became possible.[23,24)] The tunneling at a finite-length CN[25)] and a connection of different CN's[26−29)] were calculated. The conductivity was calculated also in a constant-relaxation-time approximation in the absence of a perpendicular magnetic field.[30)]

The conductivity of CN's was previously calculated using the Boltzmann transport equation[31)] and in Landauer' approach[32)] for a model of short-range scatterers. In this paper, we shall study the impurity scattering in CN's more carefully. In §2 an effective-mass Hamiltonian is derived in the presence of an impurity potential and its properties are discussed. In §3, scattering probabilities are calculated explicitly for metallic CN's both in the presence and in the absence of a magnetic field. The absence of back scattering is demonstrated for scatterers having a range comparable to or larger than the lattice constant in §4. A summary and conclusion are given in §5.

§2. Effective-Mass Equation

The structure of a two-dimensional (2D) graphite is shown in Fig. 1 together with the first Brillouin zone and the coordinates system to be used in the following. In a 2D graphite, two bands having approximately a linear dispersion cross the Fermi level (chosen at $\varepsilon=0$) at K and K' points of the first Brillouin Zone. The wave vectors of the K and K' points are given by $\boldsymbol{K}=(2\pi/a)(1/3,1/\sqrt{3})$ and $\boldsymbol{K}'=(2\pi/a)(2/3,0)$. For states in the vicinity of $\varepsilon=0$, the amplitude of the wavefunction at $\boldsymbol{R}_A$ of a site A and $\boldsymbol{R}_B$ of site B is written as

$$\begin{cases}\psi_A(\boldsymbol{R}_A)=\exp(\mathrm{i}\boldsymbol{K}\cdot\boldsymbol{R}_A)F_A^K(\boldsymbol{R}_A)+\mathrm{e}^{\mathrm{i}\eta}\exp(\mathrm{i}\boldsymbol{K}'\cdot\boldsymbol{R}_A)F_A^{K'}(\boldsymbol{R}_A),\\ \psi_B(\boldsymbol{R}_B)=-\omega\mathrm{e}^{\mathrm{i}\eta}\exp(\mathrm{i}\boldsymbol{K}\cdot\boldsymbol{R}_B)F_B^K(\boldsymbol{R}_B)+\exp(\mathrm{i}\boldsymbol{K}'\cdot\boldsymbol{R}_B)F_B^{K'}(\boldsymbol{R}_B),\end{cases}\tag{2.1}$$

with $\omega=\exp(2\pi\mathrm{i}/3)$, where η is the angle between the chiral vector $\boldsymbol{L}$ and the x' direction fixed on the graphite plane, and F_A^K, F_B^K, $F_A^{K'}$, and $F_B^{K'}$ are envelope functions assumed to be slowly-varying in the scale of the lattice constant a.

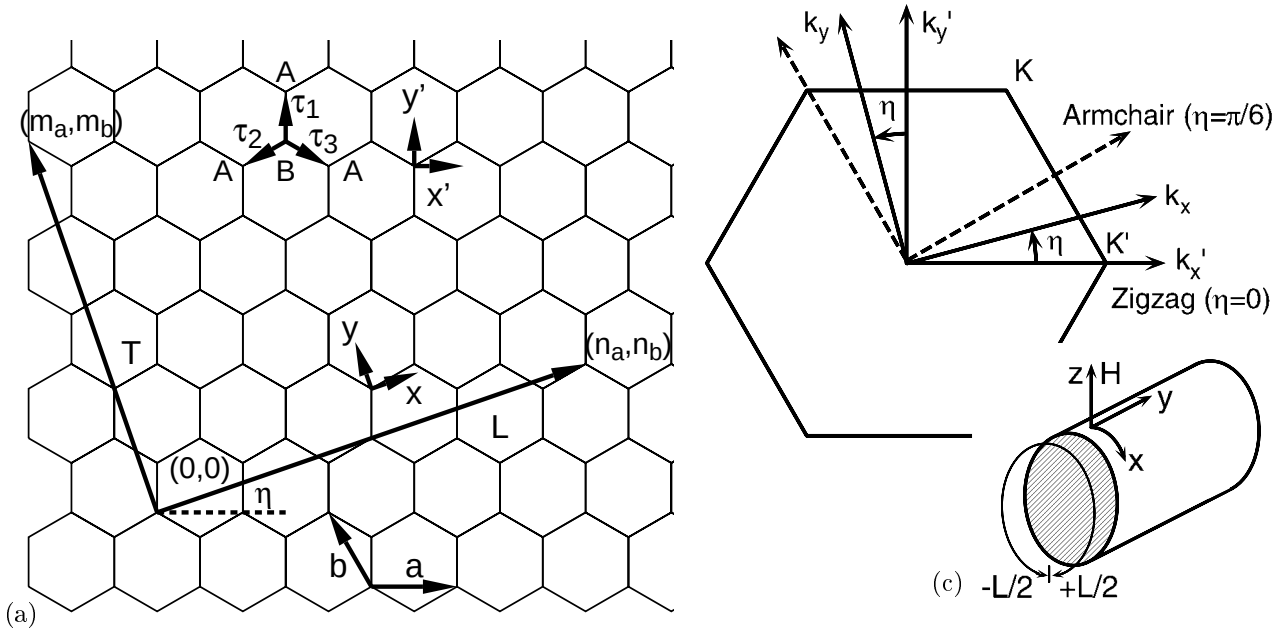

Fig. 1 (a) Lattice structure of two-dimensional graphite sheet. The coordinates (x', y') are fixed on the graphite sheet and (x, y) are chosen in such a way that x is along the circumference of a nanotube and y is along the axis. (b) The first Brillouin zone and K and K' points. (c) The coordinates for a nanotube.

We have $\boldsymbol{R}_A = n_a\boldsymbol{a}+n_b\boldsymbol{b}+\vec{\tau}$ and $\boldsymbol{R}_B = n_a\boldsymbol{a}+n_b\boldsymbol{b}$, where $\boldsymbol{a}=a(1,0)$, $\boldsymbol{b}=a(-1/2,\sqrt{3}/2)$, $\vec{\tau}=\vec{\tau}_3=a(1/2,-1/2\sqrt{3})$, and n_a and n_b are integers. We define also $\vec{\tau}_1$ and $\vec{\tau}_2$ as shown in Fig. 1(a), where $\vec{\tau}_1=a(0,1/\sqrt{3})$ and $\vec{\tau}_2=a(-1/2,-1/2\sqrt{3})$.

In the nearest-neighbor tight-binding approximation, the equation of motion for site A is given by

$$[\varepsilon-\tilde{u}_A(\boldsymbol{R}_A)]\psi_A(\boldsymbol{R}_A) = -\gamma_0\sum_{l=1}^{3}\psi_B(\boldsymbol{R}_A-\vec{\tau}_l), \tag{2.2}$$

where γ_0 is the transfer integral and $\tilde{u}_A(\boldsymbol{R}_A)$ is the local site energy. When we substitute eq. (2.1) into the above equation and use the slowly-varying nature of the envelope functions, we have

$$\begin{aligned}&[\varepsilon-\tilde{u}_A(\boldsymbol{R}_A)]\big(\mathrm{e}^{\mathrm{i}\boldsymbol{K}\cdot\boldsymbol{R}_A}F_A^K(\boldsymbol{R}_A)+\mathrm{e}^{\mathrm{i}\eta}\mathrm{e}^{\mathrm{i}\boldsymbol{K}'\cdot\boldsymbol{R}_A}F_A^{K'}(\boldsymbol{R}_A)\big)\\ =&\mathrm{e}^{\mathrm{i}\boldsymbol{K}\cdot\boldsymbol{R}_A}\gamma\mathrm{e}^{\mathrm{i}\eta}(\hat{k}'_x-\mathrm{i}\hat{k}'_y)F_B^K(\boldsymbol{R}_A)+\mathrm{e}^{\mathrm{i}\boldsymbol{K}'\cdot\boldsymbol{R}_A}\gamma(\hat{k}'_x+\mathrm{i}\hat{k}'_y)F_B^{K'}(\boldsymbol{R}_A),\end{aligned} \tag{2.3}$$

with $\gamma=(\sqrt{3}/2)a\gamma_0$ and $\hat{\boldsymbol{k}}'=-\mathrm{i}\vec{\nabla}'$.

In order to derive a Schrödinger equation for the envelopes at the K point, we first rewrite the above as

$$\begin{aligned}&[\varepsilon-\tilde{u}_A(\boldsymbol{R}_A)]\big[F_A^K(\boldsymbol{R}_A)+\mathrm{e}^{\mathrm{i}\eta}\mathrm{e}^{\mathrm{i}(\boldsymbol{K}'-\boldsymbol{K})\cdot\boldsymbol{R}_A}F_A^{K'}(\boldsymbol{R}_A)\big]\\ =&\gamma\mathrm{e}^{\mathrm{i}\eta}(\hat{k}'_x-\mathrm{i}\hat{k}'_y)F_B^K(\boldsymbol{R}_A)+\mathrm{e}^{\mathrm{i}(\boldsymbol{K}'-\boldsymbol{K})\cdot\boldsymbol{R}_A}\gamma(\hat{k}'_x+\mathrm{i}\hat{k}'_y)F_B^{K'}(\boldsymbol{R}_A).\end{aligned} \tag{2.4}$$

Introduce a function $g(\boldsymbol{R})$ normalized in such a way that

$$\sum_{\boldsymbol{R}} g(\boldsymbol{R}) = 1. \tag{2.5}$$

We assume that $g(\boldsymbol{R})$ is real, has an appreciable amplitude in the region where $|\boldsymbol{R}|$ is smaller than a few times of the lattice constant, and decays rapidly with increasing $|\boldsymbol{R}|$. This means that spatial variation of envelope functions in this region can be safely neglected. Multipling both sides of eq. (2.4) by $g(\boldsymbol{R}-\boldsymbol{R}_A)$ and summing over $\boldsymbol{R}_A$, we have

$$\varepsilon F_A^K(\boldsymbol{R}) = \gamma\mathrm{e}^{\mathrm{i}\eta}(\hat{k}'_x-\mathrm{i}\hat{k}'_y)F_B^K(\boldsymbol{R})+u_A(\boldsymbol{R})F_A^K(\boldsymbol{R})+\mathrm{e}^{\mathrm{i}\eta}u'_A(\boldsymbol{R})F_A^{K'}(\boldsymbol{R}), \tag{2.6}$$

with

$$u_A(\boldsymbol{R}) = \sum_{\boldsymbol{R}_A} g(\boldsymbol{R}-\boldsymbol{R}_A)\tilde{u}_A(\boldsymbol{R}_A), \tag{2.7}$$

and

$$u'_A(\boldsymbol{R}) = \sum_{\boldsymbol{R}_A} g(\boldsymbol{R}-\boldsymbol{R}_A)\mathrm{e}^{\mathrm{i}(\boldsymbol{K}'-\boldsymbol{K})\cdot\boldsymbol{R}_A}\tilde{u}_A(\boldsymbol{R}_A). \tag{2.8}$$

Similarly, the Schrödinger equation for the envelopes at the K' point is obtained as

$$\varepsilon F_A^{K'}(\boldsymbol{R}) = \gamma e^{-i\eta}(\hat{k}'_x + i\hat{k}'_y)F_B^{K'}(\boldsymbol{R}) + u_A(\boldsymbol{R})F_A^{K'}(\boldsymbol{R}) + e^{-i\eta}u'_A(\boldsymbol{R})^* F_A^K(\boldsymbol{R}). \tag{2.9}$$

The equation of motion for site B is given by

$$[\varepsilon - \tilde{u}_B(\boldsymbol{R}_B)]\psi_B(\boldsymbol{R}_B) = -\gamma_0 \sum_{l=1}^{3} \psi_A(\boldsymbol{R}_B + \vec{\tau}_l), \tag{2.10}$$

where $\tilde{u}_B(\boldsymbol{R}_B)$ is the local site energy. The Schrödinger equation is derived as

$$\varepsilon F_B^K(\boldsymbol{R}) = \gamma e^{-i\eta}(\hat{k}'_x + i\hat{k}'_y)F_A^K(\boldsymbol{R}) + u_B(\boldsymbol{R})F_B^K(\boldsymbol{R}) - \omega^{-1}e^{-i\eta}u'_B(\boldsymbol{R})F_B^{K'}(\boldsymbol{R}), \tag{2.11}$$

and

$$\varepsilon F_B^{K'}(\boldsymbol{R}) = \gamma e^{i\eta}(\hat{k}'_x - i\hat{k}'_y)F_A^{K'}(\boldsymbol{R}) + u_B(\boldsymbol{R})F_B^{K'}(\boldsymbol{R}) - \omega e^{i\eta}u'_B(\boldsymbol{R})^* F_B^K(\boldsymbol{R}), \tag{2.12}$$

with

$$u_B(\boldsymbol{R}) = \sum_{\boldsymbol{R}_B} g(\boldsymbol{R} - \boldsymbol{R}_B)\tilde{u}_B(\boldsymbol{R}_B), \tag{2.13}$$

and

$$u'_B(\boldsymbol{R}) = \sum_{\boldsymbol{R}_B} g(\boldsymbol{R} - \boldsymbol{R}_B)e^{i(\boldsymbol{K}'-\boldsymbol{K})\cdot\boldsymbol{R}_B}\tilde{u}_B(\boldsymbol{R}_B). \tag{2.14}$$

In summary, the effective-mass equation in the presence of an impurity potential is written as

$$\begin{pmatrix} u_A(\boldsymbol{r}) & \gamma(\hat{k}_x - i\hat{k}_y) & e^{i\eta}u'_A(\boldsymbol{r}) & 0 \\ \gamma(\hat{k}_x + i\hat{k}_y) & u_B(\boldsymbol{r}) & 0 & -\omega^{-1}e^{-i\eta}u'_B(\boldsymbol{r}) \\ e^{-i\eta}u'_A(\boldsymbol{r})^* & 0 & u_A(\boldsymbol{r}) & \gamma(\hat{k}_x + i\hat{k}_y) \\ 0 & -\omega e^{i\eta}u'_B(\boldsymbol{r})^* & \gamma(\hat{k}_x - i\hat{k}_y) & u_B(\boldsymbol{r}) \end{pmatrix} \begin{pmatrix} F_A^K(\boldsymbol{r}) \\ F_B^K(\boldsymbol{r}) \\ F_A^{K'}(\boldsymbol{r}) \\ F_B^{K'}(\boldsymbol{r}) \end{pmatrix} = \varepsilon \begin{pmatrix} F_A^K(\boldsymbol{r}) \\ F_B^K(\boldsymbol{r}) \\ F_A^{K'}(\boldsymbol{r}) \\ F_B^{K'}(\boldsymbol{r}) \end{pmatrix}, \tag{2.15}$$

where use has been made of the relation:

$$\hat{k}_x \pm i\hat{k}_y = e^{\mp i\eta}(\hat{k}'_x \pm i\hat{k}'_y), \tag{2.16}$$

and the effective potentials are given by eqs. (2.7), (2.8), (2.13), and (2.14) except that $\boldsymbol{R}$ should be replaced by the continuous variable $\boldsymbol{r}$. In a magnetic field, we have to replace $\hat{\boldsymbol{k}}$ by $-i\vec{\nabla} + e\boldsymbol{A}/\hbar c$ with vector potential $\boldsymbol{A}$.

When the impurity potential has a range larger than the lattice constant, we have $u_A(\boldsymbol{R}) = u_B(\boldsymbol{R})$. Further, $u'_A(\boldsymbol{R})$ and $u'_B(\boldsymbol{R})$ become much smaller and can be neglected because of the phase factor $e^{i(\boldsymbol{K}'-\boldsymbol{K})\cdot\boldsymbol{R}_A}$ and $e^{i(\boldsymbol{K}'-\boldsymbol{K})\cdot\boldsymbol{R}_B}$ in eqs. (2.8) and (2.14). This means that intervalley scattering between K and K' points can be neglected for such impurities. This corresponds to the limit of the usual $\boldsymbol{k}\cdot\boldsymbol{p}$ approximation where the impurity potential is incorporated as a diagonal matrix with equal elements.[33]

When the potential range is shorter than the lattice constant, we can safely replace the potentials in eq. (2.15) by delta potentials, because they have a range determined by $g(\boldsymbol{R})$ which is much shorter than the electron wave length, i.e.,

$$\begin{aligned} u_A(\boldsymbol{r}) &= u_A\delta(\boldsymbol{r} - \boldsymbol{r}_0), \\ u'_A(\boldsymbol{r}) &= u'_A\delta(\boldsymbol{r} - \boldsymbol{r}_0), \\ u_B(\boldsymbol{r}) &= u_B\delta(\boldsymbol{r} - \boldsymbol{r}_0), \\ u'_B(\boldsymbol{r}) &= u'_B\delta(\boldsymbol{r} - \boldsymbol{r}_0), \end{aligned} \tag{2.17}$$

with

$$\begin{aligned} u_A &= \frac{\sqrt{3}a^2}{2}\sum_{\boldsymbol{R}_A}\tilde{u}_A(\boldsymbol{R}_A), \\ u'_A &= \frac{\sqrt{3}a^2}{2}\sum_{\boldsymbol{R}_A} e^{i(\boldsymbol{K}'-\boldsymbol{K})\cdot\boldsymbol{R}_A}\tilde{u}_A(\boldsymbol{R}_A), \\ u_B &= \frac{\sqrt{3}a^2}{2}\sum_{\boldsymbol{R}_B}\tilde{u}_B(\boldsymbol{R}_B), \\ u'_B &= \frac{\sqrt{3}a^2}{2}\sum_{\boldsymbol{R}_B} e^{i(\boldsymbol{K}'-\boldsymbol{K})\cdot\boldsymbol{R}_B}\tilde{u}_B(\boldsymbol{R}_B), \end{aligned} \tag{2.18}$$

where $\sqrt{3}a^2/2$ is the area of a unit cell and $\boldsymbol{r}_0$ is the impurity position.

Consider an impurity potential with its center at a B site (chosen at the origin, for example) and symmetric under a 120° rotation. An A site can be represented as $n_a\boldsymbol{a} + n_b\boldsymbol{b} + \vec{\tau}_3$. For this lattice point, we have $n_a\boldsymbol{b} - n_b(\boldsymbol{a}+\boldsymbol{b}) + \vec{\tau}_2$ and $-n_a(\boldsymbol{a}+\boldsymbol{b}) + n_b\boldsymbol{a} + \vec{\tau}_1$ corresponding to +120° and −120° rotation around the origin. We have

$$\begin{aligned} (\boldsymbol{K}'-\boldsymbol{K})\cdot(n_a\boldsymbol{a} + n_b\boldsymbol{b}) &= \frac{2\pi}{3}(n_a + n_b) \pmod{2\pi}, \\ (\boldsymbol{K}'-\boldsymbol{K})\cdot[n_a\boldsymbol{b} - n_b(\boldsymbol{a}+\boldsymbol{b})] &= \frac{2\pi}{3}(n_a + n_b) \pmod{2\pi}, \\ (\boldsymbol{K}'-\boldsymbol{K})\cdot[-n_a(\boldsymbol{a}+\boldsymbol{b}) + n_b\boldsymbol{a}] &= \frac{2\pi}{3}(n_a + n_b) \pmod{2\pi}, \end{aligned} \tag{2.19}$$

and

$$(\boldsymbol{K}'-\boldsymbol{K})\cdot\vec{\tau}_1 = -\frac{2\pi}{3},$$
$$(\boldsymbol{K}'-\boldsymbol{K})\cdot\vec{\tau}_2 = 0, \tag{2.20}$$
$$(\boldsymbol{K}'-\boldsymbol{K})\cdot\vec{\tau}_3 = +\frac{2\pi}{3}.$$

These show immediately that u'_A vanishes identically while u'_B remains nonzero. In fact, when the potential is localized only at a B site, we have $u'_B = u_B$ and $u_A = u'_A = 0$.

§3. Scattering Probabilities

3.1 Metallic nanotubes in magnetic fields

We consider a metallic nanotube with circumference L in the presence of a magnetic field H perpendicular to the axis direction. The coordinate system is shown in Fig. 1(c). The energy levels and wavefunctions are analytically obtained for $\varepsilon \sim 0$ in this case.[32] The results for the gauge

$$\boldsymbol{A} = \Big(0, \frac{LH}{2\pi}\sin\frac{2\pi x}{L}\Big), \tag{3.1}$$

are

$$\boldsymbol{F}^K_{sk} = \frac{1}{\sqrt{2A}}\begin{pmatrix} -\mathrm{i}s(k/|k|)F_-(x) \\ F_+(x)\end{pmatrix}\exp(\mathrm{i}ky),$$
$$\boldsymbol{F}^{K'}_{sk} = \frac{1}{\sqrt{2A}}\begin{pmatrix} +\mathrm{i}s(k/|k|)F_+(x) \\ F_-(x)\end{pmatrix}\exp(\mathrm{i}ky), \tag{3.2}$$

with

$$F_\pm(x) = \frac{1}{\sqrt{LI_0(\alpha)}}\exp\Big[\pm\frac{1}{2}\alpha\cos\frac{2\pi x}{L}\Big], \tag{3.3}$$

where A is the length of the nanotube, $s = +1$ and -1 for the conduction and valence band, respectively, α is the parameter proportional to the magnetic field defined as

$$\alpha = 2\Big(\frac{L}{2\pi l}\Big)^2, \tag{3.4}$$

with $l = \sqrt{c\hbar/eH}$ being the magnetic length, and $I_0(z)$ is the modified Bessel function of the first kind defined as

$$I_0(z) = \int_0^\pi \frac{d\theta}{\pi}\exp(z\cos\theta). \tag{3.5}$$

In high magnetic fields ($\alpha \gg 1$), $\boldsymbol{F}_-$ is localized around $x = \pm L/2$, i.e., at the bottom side of the cylinder and $\boldsymbol{F}_+$ is localized around the top side $x = 0$. The corresponding eigenenergies are given by $\varepsilon_s(k) = s\gamma|k|I_0(\alpha)^{-1}$, which gives group velocity $v = (\gamma/\hbar)I_0(\alpha)^{-1}$ and density of states $D(0) = I_0(\alpha)/\pi\gamma$ at $\varepsilon = 0$.

Apart from the lattice constant a and effective range d of an impurity potential, the nanotubes are characterized by various length scales such as wave length $2\pi/k$ in the axis direction, wave length L in the circumference direction, and magnetic length l in strong magnetic fields. In this section we shall restrict ourselves to an impurity potential whose range is much smaller than these length scales, i.e., $d \ll 2\pi/k$, $d \ll L$, and $d \ll l$. In this case the effective potential is replaced by delta potentials given by eq. (2.17).

The matrix elements for an impurity located at $\boldsymbol{r} = \boldsymbol{r}_0$ are calculated as

$$V_{K\pm K+} = \frac{1}{2A}[\pm u_A F_-(x_0)^2 + u_B F_+(x_0)^2],$$
$$V_{K'\pm K'+} = \frac{1}{2A}[\pm u_A F_+(x_0)^2 + u_B F_-(x_0)^2],$$
$$V_{K'\pm K+} = \frac{1}{2A}[\mp u'^*_A \mathrm{e}^{-\mathrm{i}\eta} - \omega\mathrm{e}^{\mathrm{i}\eta}u'^*_B]F_+(x_0)F_-(x_0),$$
$$V_{K\pm K'+} = \frac{1}{2A}[\mp u'_A \mathrm{e}^{\mathrm{i}\eta} - \omega^{-1}\mathrm{e}^{-\mathrm{i}\eta}u'_B]F_+(x_0)F_-(x_0). \tag{3.6}$$

Averaging over the impurity position, we have

$$\langle|V_{K\pm K+}|^2\rangle = \langle|V_{K'\pm K'+}|^2\rangle = \frac{1}{A^2L^2}\frac{1}{4I_0(\alpha)^2}\big[u_A^2 I_0(2\alpha) + u_B^2 I_0(2\alpha) \pm 2u_A u_B\big],$$
$$\langle|V_{K'\pm K+}|^2\rangle = \langle|V_{K\pm K'+}|^2\rangle = \frac{1}{A^2L^2}\frac{1}{4I_0(\alpha)^2}\big[|u'_A|^2 + |u'_B|^2 \pm 2\mathrm{Re}(\omega\mathrm{e}^{2\mathrm{i}\eta}u'_A u'^*_B)\big]. \tag{3.7}$$

This shows that the scattering probabilities do not depend on the structure, i.e., on η, for scatterers with the symmetry under 120° rotations, because $u'_A u'^*_B = 0$ as discussed in the previous section.

The Boltzmann conductivity is calculated in the procedure discussed in a previous paper.[31] When we assume equal amount of scatterers at A and B sites, the results are

$$\sigma = \frac{\mathrm{e}^2}{2\pi\hbar}\Lambda, \tag{3.8}$$

with a mean free path

$$\Lambda = \frac{2\hbar^2 v^2 I_0(\alpha)}{n_i[(\langle u_A^2\rangle + \langle u_B^2\rangle)I_0(2\alpha) - 2\langle u_A u_B\rangle + \langle|u'_A|^2\rangle + \langle|u'_B|^2\rangle - 2\mathrm{Re}(\omega\mathrm{e}^{\mathrm{i}\eta}\langle u'_A u'^*_B\rangle)]}, \tag{3.9}$$

where n_i is the impurity concentration per unit area and $\langle\cdots\rangle$ represents an average over impurities. In the limit $d/a \ll 1$, in particular, we have

$$\sigma = \sigma_0\frac{2}{I_0(2\alpha)+1}, \tag{3.10}$$

with

$$\sigma_0 = \frac{\mathrm{e}^2}{2\pi\hbar}\Lambda, \quad \Lambda = \frac{\tau\gamma}{\hbar}, \quad \frac{\hbar}{\tau} = \frac{4n_i\langle u^2\rangle}{\gamma L}, \tag{3.11}$$

where $\langle u^2\rangle = \langle u_A^2\rangle = \langle|u'_A|^2\rangle = \langle u_B^2\rangle = \langle|u'_B|^2\rangle$.

Consider the case that $d/a > 1$ where $u_A = u_B$

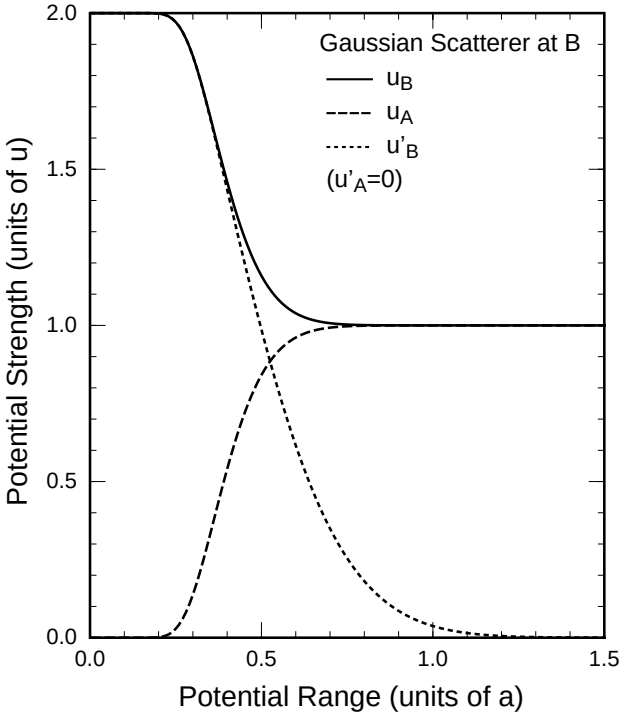

Fig. 2 Calculated effective strength of the potential for a model Gaussian impurity at a B site.

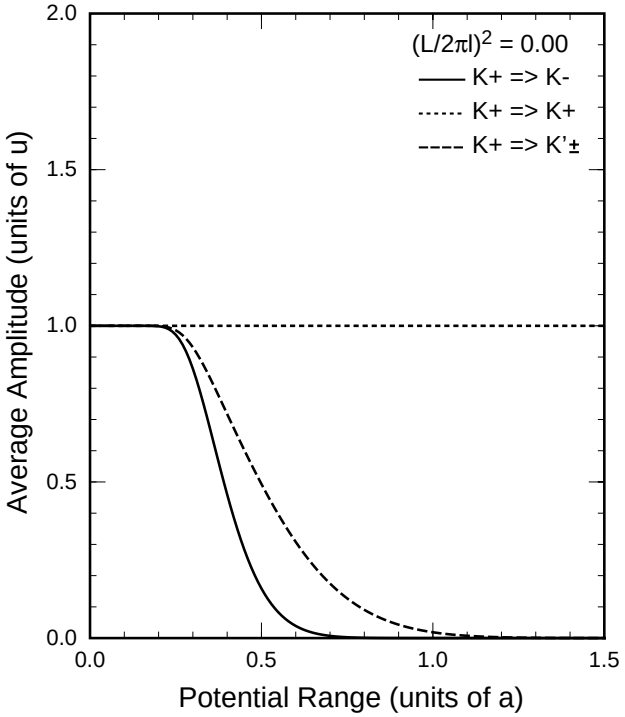

Fig. 3 Calculated effective scattering matrix elements versus the potential range at $\varepsilon = 0$ in the absence of a magnetic field.

and $u'_A = u'_B = 0$. In the absence of a magnetic field, $F_+(x_0) = F_-(x_0) = 1/\sqrt{L}$ and the back scattering matrix-elements V_{K-K+}, V_{K+K-}, $V_{K'-K'+}$, and $V_{K'+K'-}$ vanish identically together with intervalley matrix elements. This leads to an interesting and important conclusion that both mean free path and conductivity become infinitely large, $\Lambda \to \infty$ and $\sigma \to \infty$. This absence of the back scattering will be discussed further in a following section.

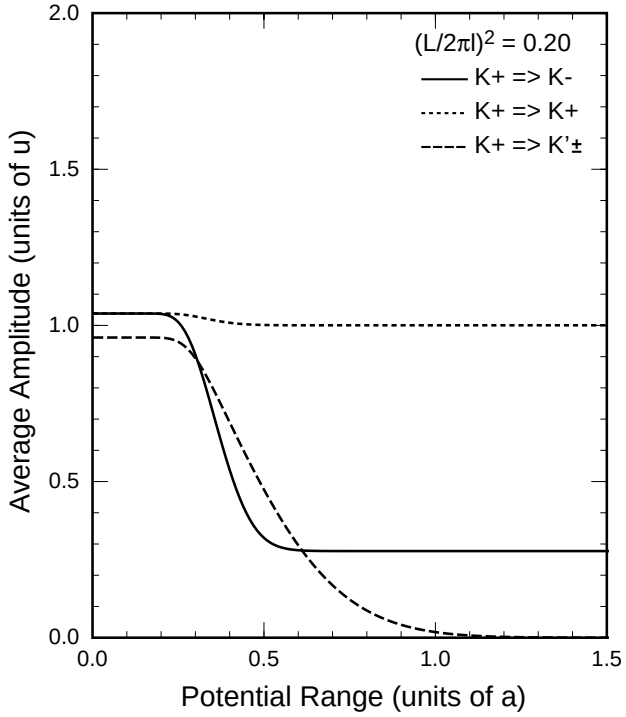

Fig. 4 Calculated effective scattering matrix elements versus the potential range at $\varepsilon = 0$ in magnetic field $(L/2\pi l)^2 = 0.2$.

3.2 Model impurity

As a model of a scatterer, we consider a Gaussian potential with its center at a B site and its range d such that $d \ll L$. The potential is given by

$$V(r) = \frac{f(d/a)u}{\pi d^2} \exp\Big(-\frac{r^2}{d^2}\Big), \tag{3.12}$$

where $f(d/a)$ is determined by the normalization condition:

$$\sum_{\boldsymbol{R}} \frac{\sqrt{3}a^2}{4} \frac{f(d/a)}{\pi d^2} \Big[\exp\Big(-\frac{\boldsymbol{R}^2}{d^2}\Big) + \exp\Big(-\frac{(\boldsymbol{R}+\vec{\tau})^2}{d^2}\Big)\Big] = 1. \tag{3.13}$$

The effective potential can be represented as eq. (2.17). Obviously, we have the following relations for the coefficient of the delta function:

$$\begin{aligned} u_A + u_B &= 2u, \\ u'_A &= 0. \end{aligned} \tag{3.14}$$

In the limit of short-range scatterers, i.e., $d \ll a$, we have

$$u_A = 0, \quad u_B = 2u, \quad u'_A = 0, \quad u'_B = 2u. \tag{3.15}$$

In the limit of long-range scatterers, i.e., $d \gg a$, on the other hand, we have

$$u_A = u, \quad u_B = u, \quad u'_A = 0, \quad u'_B = 0. \tag{3.16}$$

3.3 Numerical results

Figure 2 gives an example of calculated effective potential u_A, u_B, and u'_B as a function of d/a for a Gaussian potential located at a B site. As has been mentioned, we have $u'_A = 0$ independent of d/a. When the range is sufficiently small, u_B and u'_B stay close to $2u$ because the potential is localized only at the impurity

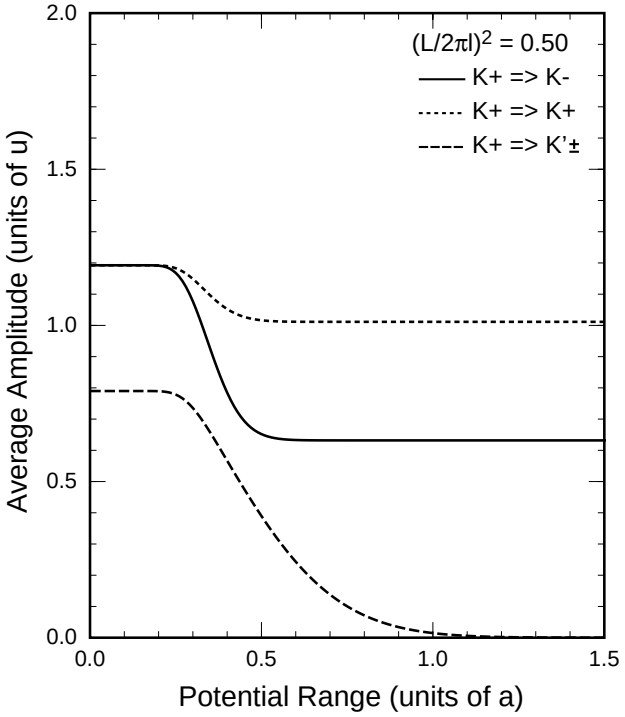

Fig. 5 Calculated effective scattering matrix elements versus the potential range at $\varepsilon = 0$ in magnetic field $(L/2\pi l)^2 = 0.5$.

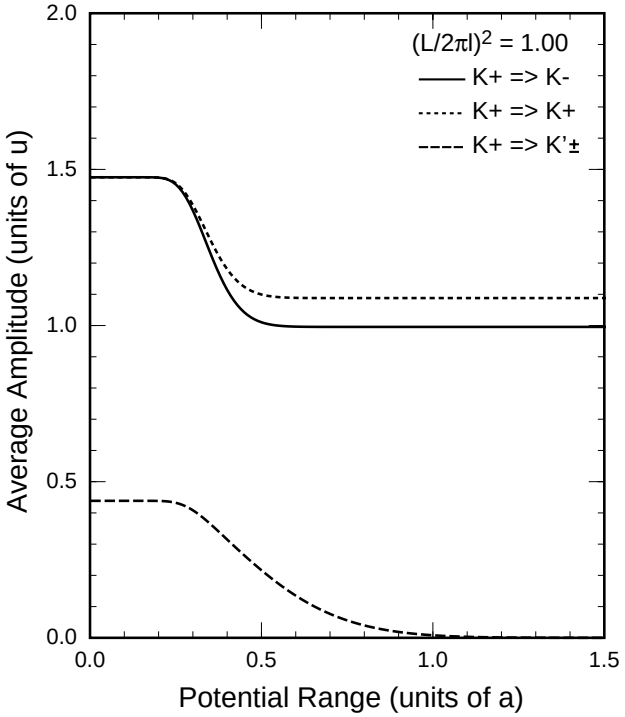

Fig. 6 Calculated effective scattering matrix elements versus the potential range at $\varepsilon = 0$ in magnetic field $(L/2\pi l)^2 = 1$.

B site. With the increase of d the potential becomes nonzero even at neighboring A sites and u_A starts to increase and at the same time both u_B and u'_B decrease. The diagonal elements u_A and u_B rapidly approach u and the off-diagonal element u'_B vanishes more slowly. The same results can be obtained for an impurity at an A site if we exchange A and B in the above.

Figure 3 shows calculated averaged scattering amplitude, defined as $AL\sqrt{\langle|V_{K\pm K+}|^2\rangle}$ and $AL\sqrt{\langle|V_{K'\pm K+}|^2\rangle}$ where $\langle|V_{K\pm K+}|^2\rangle$ and $\langle|V_{K'\pm K+}|^2\rangle$ are defined in eq. (3.7), as a function of d in the absence of a magnetic field. The back scattering probability decreases rapidly with d and becomes exponentially small for $d/a \gg 1$. The same is true of the intervalley scattering although the dependence is slightly weaker because of the slower decrease of u'_B shown in Fig. 2.

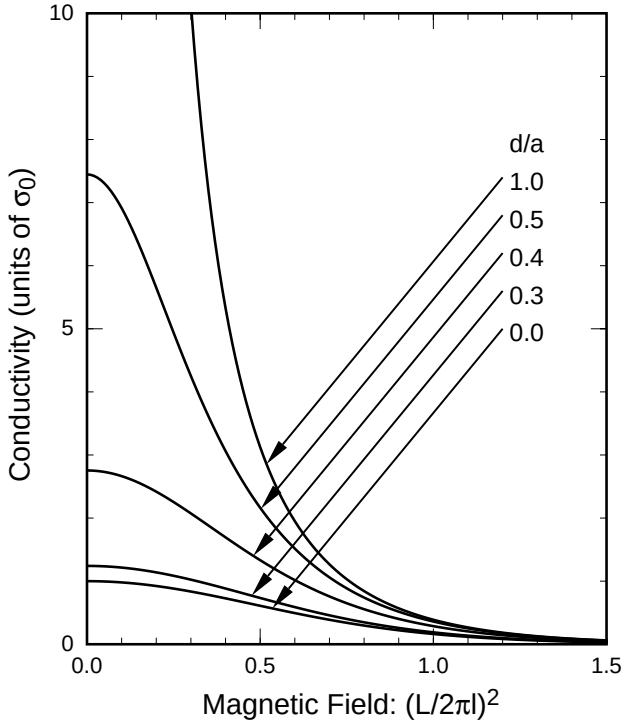

Fig. 7 Calculated conductivity at $\varepsilon = 0$ as a function of the effective magnetic field for various values of d/a. At $(L/2\pi l)^2 = 0$, the conductivity becomes extremely large for $d/a > 1$.

This singular behavior disappears in the presence of magnetic fields as shown in Figs. 4, 5, and 6. In high magnetic fields, the intervalley scattering is reduced considerably because of the reduction in the overlap of the wavefunction as shown in eq. (3.2). The conductivity in the region $d/a \sim 1$ varies strongly as a function of the magnetic field.

Figure 7 gives examples of the calculated Boltzmann conductivity as a function of the effective magnetic field $(L/2\pi l)^2$. The positive magnetoresistance present even for $d/a \ll 1$ becomes stronger with the increase of d/a. The conductivity in the absence of a magnetic field is extremely large when $d/a > 1$ because of the vanishing back scattering probability.

It is straightforward to calculate a scattering matrix for an impurity given by eq. (2.17) and a conductance of a finite-length nanotube containing many impurities, combining S matrices as discussed previously.[32] Figures 8 and 9 show some examples of calculated conductance at $\varepsilon = 0$ in the case that the impurity potential has a range larger than the lattice constant, i.e., $u_A = u_B = u$. A typical mean free path Λ defined in eq. (3.11) for the present u is $\Lambda/L = 10$ in the former case and $\Lambda/L = 1$ in the latter case (the definition of Λ is actually quite ambiguous because of the singular dependence on the magnetic field). The conductance in the absence of a

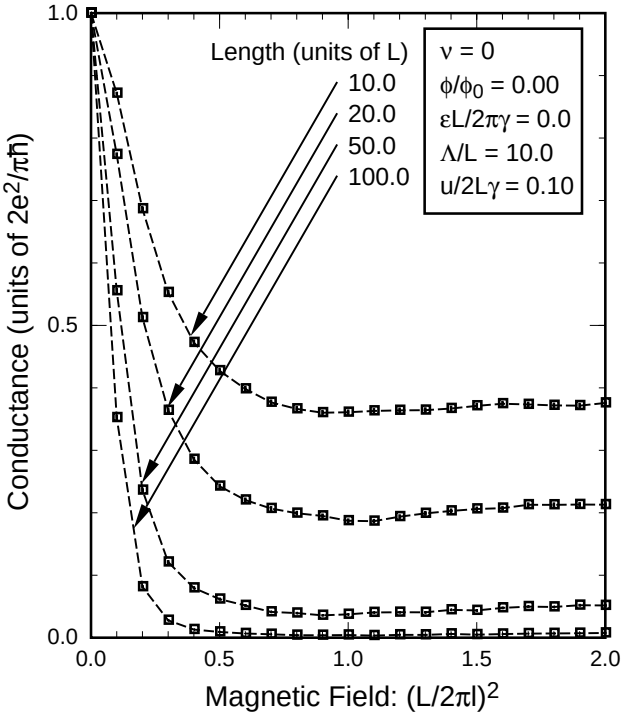

Fig. 8 Calculated conductance of finite-length nanotubes at $\varepsilon=0$ as a function of the effective strength of a magnetic field in the case that the effective mean free path is much larger than the circumference. The conductance is always given by the value in the absence of impurities at $H=0$.

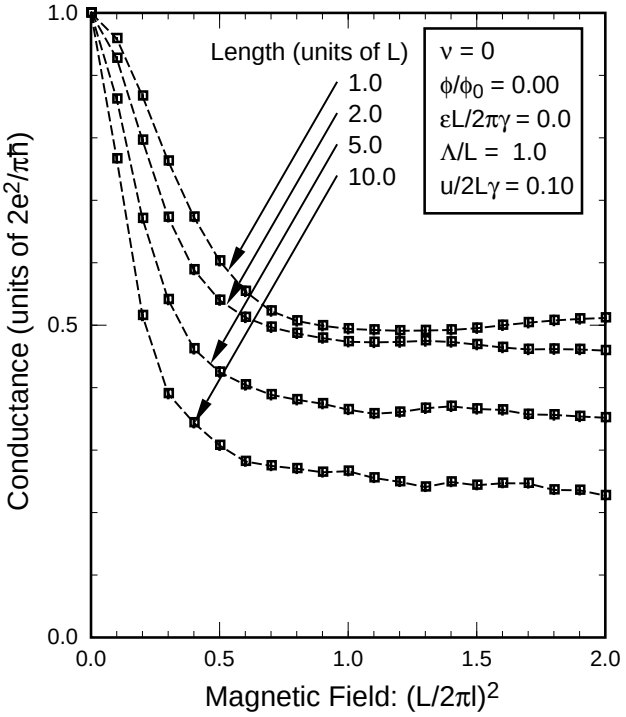

Fig. 9 Calculated conductance of finite-length nanotubes at $\varepsilon=0$ as a function of the effective strength of a magnetic field in the case that the effective mean free path is comparable to the circumference.

magnetic field is always quantized into $2e^2/\pi\hbar$ because of the complete absence of back scattering. With the increase of the magnetic field the conductance is reduced drastically and the amount of the reduction becomes larger with the increase of the length.

§4. Absence of Back Scattering

As has been shown in the previous section, the back scattering probability vanishes when the potential range exceeds the lattice constant and the effective potential for the A site is the same as that of the neighboring B site. We can show that this result is not limited to the lowest order Born approximation but is quite general in metallic nanotubes.

We consider the K point. In this case the wave function and the energy are given by

$$\begin{aligned} \boldsymbol{F}_{nsk}(\boldsymbol{r}) &= \frac{1}{\sqrt{2AL}} \begin{pmatrix} b(n,k) \\ +s \end{pmatrix} \exp\left[\mathrm{i}\kappa(n)x+\mathrm{i}ky\right], \\ \varepsilon_{ns}(k) &= s\sqrt{\kappa(n)^2+k^2}, \end{aligned} \tag{4.1}$$

with

$$\begin{aligned} b(n,k) &= \frac{\kappa(n)-\mathrm{i}k}{\sqrt{\kappa(n)^2+k^2}}, \\ \kappa(n) &= \frac{2\pi}{L}n, \end{aligned} \tag{4.2}$$

where n is an integer. In particular, for $n=0$, $s=+1$, and $k>0$, we have

$$\boldsymbol{F}_{0+k}(\boldsymbol{r}) = \frac{1}{\sqrt{2AL}} \begin{pmatrix} -\mathrm{i}k/|k| \\ 1 \end{pmatrix} \exp(\mathrm{i}ky). \tag{4.3}$$

Consider a T matrix defined by

$$T = V + V\frac{1}{\varepsilon-\mathcal{H}_0}V + V\frac{1}{\varepsilon-\mathcal{H}_0}V\frac{1}{\varepsilon-\mathcal{H}_0}V + \cdots, \tag{4.4}$$

where V is the impurity potential which is just a scalar because it is same for both A and B sites, ε is the energy, and $\mathcal{H}_0$ is the Hamiltonian in the absence of the impurity. We consider the matrix

$$\hat{T} = \begin{pmatrix} T_{++} & T_{+-} \\ T_{-+} & T_{--} \end{pmatrix}, \tag{4.5}$$

where T_{++} represents the matrix element for the scattering within the state with positive wave vector $+k$ along the axis direction for the band index $n=0$ and $s=+1$ (conduction band), T_{+-} from $-k$ to $+k$, T_{-+} from $+k$ to $-k$, and T_{--} within $-k$.

The matrix element of the impurity potential is given by

$$\begin{aligned} (nsk|V|n's'k') =& \frac{1}{AL}V_{n-n'}(k-k') \\ & \times \frac{1}{2}\left(b(n,k)^* \quad s\right) \begin{pmatrix} b(n',k') \\ s' \end{pmatrix}, \end{aligned} \tag{4.6}$$

with

$$V_n(k) = \int dx \int dy\, V(x,y) \exp\left[-\mathrm{i}\kappa(n)x-\mathrm{i}ky\right]. \tag{4.7}$$

Therefore, the lowest order term becomes

$$\begin{aligned} \hat{T}^{(1)} &= \frac{1}{AL}V_0[(\pm k)-(\pm k)]\, U^+U \\ &= \frac{1}{AL}V_0[(\pm k)-(\pm k)] \begin{pmatrix} 1 & 0 \\ 0 & 1 \end{pmatrix}, \end{aligned} \tag{4.8}$$

with

$$U = \frac{1}{\sqrt{2}} \begin{pmatrix} -\mathrm{i} & \mathrm{i} \\ 1 & 1 \end{pmatrix}. \tag{4.9}$$

This shows the vanishing of the back scattering matrix element in the lowest order.

The second order term is written as

$$\hat{T}^{(2)} = \frac{1}{AL}\frac{1}{AL}\sum_{n_1 k_1} \frac{V_{-n_1}[(\pm k)-k_1]V_{n_1}[k_1-(\pm k)]}{\varepsilon_{0+}(k)-\varepsilon_{n_1 s_1}(k_1)} \times [1-s_1(\boldsymbol{n}(n_1,k_1)\cdot\vec{\sigma})], \tag{4.10}$$

where $\boldsymbol{n}=(n_x,n_y,n_z)$ is a unit vector defined as

$$\begin{aligned} n_x(n,k) &= 0, \\ n_y(n,k) &= \frac{\kappa(n)}{\sqrt{\kappa(n)^2+k^2}}, \\ n_z(n,k) &= \frac{k}{\sqrt{\kappa(n)^2+k^2}}, \end{aligned} \tag{4.11}$$

and $\vec{\sigma}=(\sigma_x,\sigma_y,\sigma_z)$ is the Pauli spin matrix. In the above use has been made of

$$U^+ \begin{pmatrix} b(n,k) \\ s \end{pmatrix} (b(n,k)^* \quad s) U = 1-s(\boldsymbol{n}(n,k)\cdot\vec{\sigma}). \tag{4.12}$$

It is easy to show that the off-diagonal element of $T^{(2)}$ vanishes after being summed for pair states (s_1,n_1,k_1) and $(s_1,-n_1,-k_1)$. In fact, under the transformation $(s_1,n_1,k_1)\to(s_1,-n_1,-k_1)$, both energy denominator and potential matrix elements are invariant while the off-diagonal elements of eq. (4.12) change their signature.

The next order term is give by

$$\begin{aligned} \hat{T}^{(3)} =& \frac{1}{AL}\frac{1}{AL}\sum_{n_1 k_1}\frac{1}{AL}\sum_{n_2 k_2} \\ & \times \frac{V_{-n_1}[(\pm k)-k_1]V_{n_1-n_2}(k_1-k_2)V_{n_2}[k_2-(\pm k)]}{[\varepsilon_{0+}(k)-\varepsilon_{n_1 s_1}(k_1)][\varepsilon_{0+}(k)-\varepsilon_{n_2 s_2}(k_2)]} \\ & \times [1-s_1(\boldsymbol{n}_1\cdot\vec{\sigma})][1-s_2(\boldsymbol{n}_2\cdot\vec{\sigma})], \end{aligned} \tag{4.13}$$

where

$$\boldsymbol{n}_j = \boldsymbol{n}(n_j,k_j). \tag{4.14}$$

If we note that

$$(\boldsymbol{n}_1\cdot\vec{\sigma})(\boldsymbol{n}_2\cdot\vec{\sigma}) = (\boldsymbol{n}_1\cdot\boldsymbol{n}_2) + \mathrm{i}(\boldsymbol{n}_1\times\boldsymbol{n}_2)\sigma_x, \tag{4.15}$$

with $\boldsymbol{n}_1\times\boldsymbol{n}_2 = n_{1x}n_{2y}-n_{1y}n_{2x}$, we have

$$\begin{aligned} & [1-s_1(\boldsymbol{n}_1\cdot\vec{\sigma})][1-s_2(\boldsymbol{n}_2\cdot\vec{\sigma})] \\ =& 1+s_1s_2(\boldsymbol{n}_1\cdot\boldsymbol{n}_2)-s_1(\boldsymbol{n}_1\cdot\vec{\sigma})-s_2(\boldsymbol{n}_2\cdot\vec{\sigma}) \\ & +\mathrm{i}s_1s_2(\boldsymbol{n}_1\times\boldsymbol{n}_2)\sigma_x. \end{aligned} \tag{4.16}$$

The off-diagonal elements of the above quantity change their signature when we make the exchange $(s_1,n_1,k_1)\to(s_2,-n_2,-k_2)$ and $(s_2,n_2,k_2)\to(s_1,-n_1,-k_1)$, leading immediately to vanishing of the off-diagonal elements of $\hat{T}^{(3)}$.

More generally, the $(p+1)$th order term is written as

$$\begin{aligned} \hat{T}^{(p+1)} =& \frac{1}{AL}\frac{1}{AL}\sum_{n_1 k_1}\frac{1}{AL}\sum_{n_2 k_2}\cdots\frac{1}{AL}\sum_{n_p k_p} \\ & \times \frac{V_{-n_1}[(\pm k)-k_1]V_{n_1-n_2}(k_1-k_2)\cdots V_{n_p}[k_p-(\pm k)]}{[\varepsilon_{0+}(k)-\varepsilon_{n_1 s_1}(k_1)]\cdots[\varepsilon_{0+}(k)-\varepsilon_{n_p s_p}(k_p)]} \\ & \times [1-s_1(\boldsymbol{n}_1\cdot\vec{\sigma})][1-s_2(\boldsymbol{n}_2\cdot\vec{\sigma})]\cdots[1-s_p(\boldsymbol{n}_p\cdot\vec{\sigma})]. \end{aligned} \tag{4.17}$$

As will be shown in Appendix A, the off-diagonal element of

$$(\boldsymbol{n}_1\cdot\vec{\sigma})(\boldsymbol{n}_2\cdot\vec{\sigma})\cdots(\boldsymbol{n}_q\cdot\vec{\sigma}) \tag{4.18}$$

can be shown to have a value whose sign is opposite to the off-diagonal element of

$$(-\boldsymbol{n}_q\cdot\vec{\sigma})\cdots(-\boldsymbol{n}_2\cdot\vec{\sigma})(-\boldsymbol{n}_1\cdot\vec{\sigma}), \tag{4.19}$$

for arbitrary q. This leads to the vanishing of the off-diagonal element of $\hat{T}^{(p+1)}$ by changing the variables into those obtained by the time reversal operation, $(s_1,n_1,k_1)\to(s_p,-n_p,-k_p)$, $(s_2,n_2,k_2)\to(s_{p-1},-n_{p-1},-k_{p-1})$, ... This completes the proof that no backscattering process is present for any impurity potential within the band $n=0$ in metallic nanotubes.

When the electron energy exceeds $2\pi\gamma/L$ or becomes lower than $-2\pi\gamma/L$, new scattering channels open up because of the presence of bands with $n=\pm1$. In this case the scattering into these bands makes back scattering possible, although the back scattering within the band $n=0$ is still absent, leading to a finite mean free path and conductivity.

The absence of back scattering in nanotubes corresponds to the vanishing matrix elements for back scattering in a 2D graphite sheet. In a graphite sheet, however, it does not give rise to any singular effect because the mean free path remains finite due to the presence of scattering into various other directions.[34] In nanotubes, the quantization of the electron motion perpendicular to the tube axis singles out the complete absence of back scattering, leading to an infinitely large mean free path in the absence of a magnetic field.

It is highly likely that the absence of back scattering can be explained by a much simpler argument based on some symmetry of the system and interpreted more intuitively. This problem is left for a future study, however.

§5. Summary and Discussion

In summary, we have derived effective potential of an impurity in two-dimensional graphite sheet appearing in a $\boldsymbol{k}\cdot\boldsymbol{p}$ scheme. When the potential range is smaller than the lattice constant, it has an off-diagonal matrix element between K and K' points comparable to the diagonal element. With the increase of the range, this off-diagonal element decreases rapidly and the diagonal element for envelopes at A and B sites becomes identical. The crossover between these two regimes occurs around the range smaller than the lattice constant.

When intervalley terms can be neglected and the diagonal effective potential is identical for neighboring A and B sites, the back scattering between states with $+k$ and $-k$ vanishes identically for the bands crossing the Fermi level in the absence of a magnetic field. This leads to an extremely large conductivity or mean free path. The absence of the back scattering disappears in magnetic fields, giving rise to a huge positive magnetoresistance.

There has essentially been no information on main scattering mechanisms in nanotubes. Charged impurites may give rise to a potential with a range much larger

than the lattice constant. A possible deformation or distortion of a nanotube may give rise to an effective long-range potential. The present results show that such long- or medium-range perturbatons can be neglected as scattering mechanisms in metallic nanotubes. Lattice defects such as carbon vacancies may likely give rise to a perturbation described by a strong potential with a range comparable to the lattice constant. Only such short-range scatterers can be a mechanism of limiting the mean free path and the conductivity.

The conductance of a single-wall nanotube was observed quite recently,[35] but experiments show large charging effects presumably due to nonideal contacts. It is highly desirable to become able to measure transport of a single-wall nanotube with ideal Ohmic contacts in order to observe this interesting prediction experimentally.

Acknowledgments

We thank Professor R. Saito for helpful discussions. This work was supported in part by Grant-in-Aid for Scientific Research from Ministry of Education, Science and Culture. Numerical calculations were performed in part on FACOM VPP500 in Supercomputer Center, Institute for Solid State Physics, University of Tokyo.

Appendix A: Some Properties of Spin Matrix

We define

$$P(\boldsymbol{n}_1,\ldots,\boldsymbol{n}_p) = (\boldsymbol{n}_1\cdot\vec{\sigma})(\boldsymbol{n}_2\cdot\vec{\sigma})\cdots(\boldsymbol{n}_p\cdot\vec{\sigma}). \tag{A1}$$

We consider first the case of even p. Using eq. (4.15), we first perform multiplication of pairs (1,2), (3,4), ..., and $(p-1,p)$. Then, we have

$$\begin{aligned} P(\boldsymbol{n}_1,\ldots\boldsymbol{n}_p) =&[(\boldsymbol{n}_1\cdot\boldsymbol{n}_2)+\mathrm{i}(\boldsymbol{n}_1\times\boldsymbol{n}_2)\sigma_x]\cdots \\ &\times[(\boldsymbol{n}_{p-1}\cdot\boldsymbol{n}_p)+\mathrm{i}(\boldsymbol{n}_{p-1}\times\boldsymbol{n}_p)\sigma_x] \end{aligned} \tag{A2}$$

The off-diagonal element consists of the term proportional to σ_x which is proportional to the sum of terms consisting of an odd number of $\boldsymbol{n}_j\times\boldsymbol{n}_{j+1}$. These terms change their signature when we make the transformation:

$$\boldsymbol{n}_1\to-\boldsymbol{n}_p,\quad \boldsymbol{n}_2\to-\boldsymbol{n}_{p-1},\ldots,\boldsymbol{n}_p\to-\boldsymbol{n}_1. \tag{A3}$$

This immediately shows that the off-diagonal element of P changes its signature under the above transformation.

In order to discuss the case of odd p, we first consider the product of three terms. Using eq. (4.15), we have

$$\begin{aligned} &(\boldsymbol{n}_1\cdot\vec{\sigma})(\boldsymbol{n}_2\cdot\vec{\sigma})(\boldsymbol{n}_3\cdot\vec{\sigma}) = [(\boldsymbol{n}_1\cdot\boldsymbol{n}_2)+\mathrm{i}(\boldsymbol{n}_1\times\boldsymbol{n}_2)\sigma_x](\boldsymbol{n}_3\cdot\vec{\sigma}) \\ &\quad=(\boldsymbol{n}_1\cdot\boldsymbol{n}_2)(\boldsymbol{n}_3\cdot\vec{\sigma})+(\boldsymbol{n}_3\cdot\boldsymbol{n}_2)(\boldsymbol{n}_1\cdot\vec{\sigma})-(\boldsymbol{n}_1\cdot\boldsymbol{n}_3)(\boldsymbol{n}_2\cdot\vec{\sigma}) \\ &\quad=(\boldsymbol{n}_3\cdot\vec{\sigma})(\boldsymbol{n}_2\cdot\vec{\sigma})(\boldsymbol{n}_1\cdot\vec{\sigma}). \end{aligned} \tag{A4}$$

By using this relation repeatedly, we can show that for odd p

$$\begin{aligned} P(\boldsymbol{n}_1,\boldsymbol{n}_2,\ldots,\boldsymbol{n}_p) &= P(\boldsymbol{n}_p,\ldots,\boldsymbol{n}_2,\boldsymbol{n}_1) \\ &= -P(-\boldsymbol{n}_p,\ldots,-\boldsymbol{n}_2,-\boldsymbol{n}_1). \end{aligned} \tag{A5}$$

In the case of $p=5$, for example, we have $\underline{12}345\to32\underline{145}\to\underline{325}41\to52\underline{34}1\to54321$. In the case of $p=7$, we have $\underline{1234567}\to32\underline{1476}5\to\underline{3274165}\to7234\underline{56}1\to7\underline{236}541\to76\underline{325}41\to765\underline{234}1\to7654321$. This immediately leads to the conclusion that the off-diagonal element of P changes its signature under the transformation (A3).

1) S. Iijima: Nature (London) **354** (1991) 56.
2) N. Hamada, S. Sawada, and A. Oshiyama: Phys. Rev. Lett. **68** (1992) 1579.
3) J. W. Mintmire, B. I. Dunlap, and C. T. White, Phys. Rev. Lett. **68** (1992) 631.
4) R. Saito, M. Fujita, G. Dresselhaus, and M. S. Dresselhaus: Phys. Rev. B **46** (1992) 1804.
5) R. Saito, M. Fujita, G. Dresselhaus, and M. S. Dresselhaus: Appl. Phys. Lett. **60** (1992) 2204.
6) M.S. Dresselhaus, G. Dresselhaus, and R. Saito: Phys. Rev. B **45** (1992) 6234.
7) M. S. Dresselhaus, G. Dresselhaus, R. Saito, and P. C. Eklund: *Elementary Excitations in Solids*, ed. J. L. Birman, C. Sebenne, and R. F. Wallis (Elsevier Science Publishers B.V., Amsterdam, 1992) p. 387.
8) R. A. Jishi, M. S. Dresselhaus, and G. Dresselhaus: Phys. Rev. B **47** (1993) 16671.
9) K. Tanaka, K. Okahara, M. Okada, and T. Yamabe: Chem. Phys. Lett. **191** (1992) 469.
10) Y. D. Gao and W. C. Herndon: Mol. Phys. **77** (1992) 585.
11) D. H. Robertson, D. W. Berenner, and J. W. Mintmire: Phys. Rev. B **45** (1992) 12592.
12) C. T. White, D. C. Robertson, and J. W. Mintmire: Phys. Rev. B **47** (1993) 5485.
13) H. Ajiki and T. Ando: J. Phys. Soc. Jpn. **62** (1993) 1255.
14) H. Ajiki and T. Ando: J. Phys. Soc. Jpn. **65** (1996) 505.
15) H. Ajiki and T. Ando: J. Phys. Soc. Jpn. **62** (1993) 2470; **63** (1994) 4267.
16) H. Ajiki and T. Ando: J. Phys. Soc. Jpn. **64** (1995) 4382.
17) H. Ajiki and T. Ando: Physica B **201** (1994) 349.
18) H. Ajiki and T. Ando: Jpn. J. Appl. Phys. Suppl. **34** (1995) 107.
19) T. Ando: J. Phys. Soc. Jpn. **66** (1997) 1066.
20) N. A. Viet, H. Ajiki, and T. Ando: J. Phys. Soc. Jpn. **63** (1994) 3036.
21) H. Ajiki and T. Ando: J. Phys. Soc. Jpn. **64** (1995) 260.
22) S. N. Song, X. K. Wang, R. P. H. Chang, and J. B. Ketterson: Phys. Rev. Lett. **72** (1994) 697.
23) L. Langer, V. Bayot, E. Grive, J. -P. Issi, J. P. Heremans, C. H. Olk, L. Stockman, C. Van Haesendonck, and Y. Brunseraede: Phys. Rev. Lett. **76** (1996) 479.
24) F. Katayama, Master thesis (Univ. Tokyo, 1996).
25) W. -D. Tian and S. Datta: Phys. Rev. B **49** (1994) 5097.
26) R. Saito, G. Dresselhaus, and M. S. Dresselhaus: Phys. Rev. B **53** (1996) 2044.
27) R. Tamura, and M. Tsukada: Solid State Commun. **101** (1997) 601.
28) R. Tamura, and M. Tsukada: Phys. Rev. B **55** (1997) 4991.
29) T. Nakanishi and T. Ando: J. Phys. Soc. Jpn. **66** (1997) 2973.
30) Y. Miyamoto, S. G. Louie, and M. L. Cohen, Phys. Rev. Lett. **76** (1996) 2121.
31) T. Seri and T. Ando: J. Phys. Soc. Jpn. **66** (1997)

169.
32) T. Ando and T. Seri: J. Phys. Soc. Jpn. **66** (1997) 3558.
33) J. M. Luttinger and W. Kohn, Phys. Rev. **97** (1955) 869.
34) N. H. Shon and T. Ando: J. Phys. Soc. Jpn. **67** (1998) No. 7.
35) S. J. Tans, M. H. Devoret, H. -J. Dai, A. Thess, R. E. Smalley, L. J. Geerligs, and C. Dekker: Nature **386** (1997) 474.